

NANO-ROD SUSPENSION FLOWS: A 2D SMOLUCHOWSKI-NAVIER-STOKES SOLVER

M. GREGORY FOREST, RUHAI ZHOU, AND QI WANG

(Communicated by L. Hou)

Abstract. We present a numerical algorithm for nano-rod suspension flows, and provide benchmark simulations of a plane Couette cell experiment. The system consists of a Smoluchowski equation for the orientational distribution function of the nano-rods together with the Navier-Stokes equation for the solvent with an orientation-dependent stress. The rigid rods interact through nonlocal excluded-volume and distortional elasticity potentials and hydrodynamic interactions. The algorithm resolves full orientational configuration space (a spherical harmonic Galerkin expansion), two dimensional physical space (method of lines discretization), and time (spectral deferred corrections), and employs a velocity-pressure formulation of the Navier-Stokes equation. This method extends our previous solver [25] from 1D to 2D in physical space.

Key Words. Navier-Stokes, Smoluchowski equation, numerical methods, nano-rods, suspension flow

1. Introduction

Numerical simulations are critical for smart engineering of high-performance nano-composite materials. This paper is one step toward that goal, which we briefly explain in this introduction. While traditional composite engineering is replete with sophisticated control and optimization technology, based on accurate and fast direct and inverse solvers, nano-composites still remain unresolved with respect to various stages of the direct problem. There are fundamental limiting steps that must be overcome to reach a comparable level of simulation capability; the solver presented here addresses one of those steps.

Nano-rods and nano-platelets are too numerous and too small to image in statistically sufficient detail. Consider that nano-rod and nano-platelet macromolecules at 1% volume fraction and $1nm \times 100nm$ aspect ratio consist of 10^6 or greater particles in a cubic micron. Nano-clay platelets at this composition introduce football fields of new surface area in a raindrop [22]. The key to probing these nano-scale composites is high-fidelity resolved simulations combined with sparse data to interpret the dataset, to validate the model, and to perform inverse characterization of the modeling parameters. We have not reached that level of cross-talk and confirmation between theory and experiment.

The targets of nano-composite technology are the remarkable property enhancements that have been achieved in model systems. Properties range from conductivities to permeabilities to mechanical. Post-processed properties and performance

Received by the editors March 3, 2006.

2000 *Mathematics Subject Classification.* 65N06, 65N40, 76M20.

features of nano-composite materials are a direct consequence of the orientational probability distribution (PDF) of the nano-particles; this is an empirical fact. But, *how* flow-processing, composition, and effective properties are related remains an open and difficult challenge. There are not sufficient quantities and resources to span experimental parameter space. The modeling state of affairs has been restricted to highly idealized limits where the rods or platelets are either perfectly aligned or random [19], with no ability to link the role of composition and flow to volume-averaged and percolation induced property enhancements. Our research group has made partial inroads into this problem, and the algorithms presented here take us yet another step further.

For the processing phase, the theoretical and computational obstruction is related to anisotropy: inherently due to the high aspect ratio of individual particles, but which then passes upscale to the ensemble distribution function. Otherwise, advanced sphere-viscous solvent dispersion codes would have resolved this problem long ago. Molecular dynamics simulations with parametrized Gay-Berne potentials have not yet been successful even in the homogeneous limit of orientational distributions for aspect ratios greater than 10; nano-particles typically have aspect ratios in the hundreds if not thousands. Because of nonlocal particle excluded-volume interactions, which require tracking of particle orientations with respect to their neighbors, rigid rod suspensions are extremely sensitive to low-moment closure models ([7]). This requires a resolved simulation of the Smoluchowski equation of Doi [3] and Hess [16] for the orientational probability distribution function (PDF). Following Larson and Ottinger [18], Grosso et al. [13], and Faraoni et al. [5], we first developed a Galerkin spherical harmonic expansion algorithm of the Smoluchowski equation in the longwave limit, together with a spectral deferred correction method for the dynamics. This formulation posits a linear flow, suppresses flow feedback, and computes how the PDF is modified by the coupling of excluded volume, torque and translation of spheroidal particles due to flow, and the geometry and volume fraction of the rods or platelets. With this code, we implemented continuation software (AUTO) [2] and thereby mapped out phase diagrams of PDF attractors versus linear flow type and strength, volume fraction of the rigid rods, and particle aspect ratio [9, 8, 11, 10]. Next, we generalized the method to 1D in physical space [25], allowing for hydrodynamic feedback, a fixed experimental geometry with wall confinement and driving conditions. Simulations of this code allowed us to map out space-time attractors versus flow and material elasticity parameters [12], and that numerical study continues. The output yields structure morphology in films, both in the orientational PDF of the rod ensemble and in the flow profile. Furthermore, the heterogeneous ensemble distributions are directly transferred to homogenization and new percolation methods to predict effective properties. This brings us to the present paper and the algorithms presented for 2D in physical space. With them, we can study stability of the 1D film composites to higher physical space perturbations, and we can simulate fully 2D flow and orientational structures. These are immediate applications of the algorithm developed here; for this paper, we provide only benchmark simulations.

2. Kinetic model equations

We consider an ensemble of high aspect ratio, rigid rods in a viscous solvent, confined between two parallel plates which are moving at the same speed in opposite directions. The rods are modeled as spheroids with aspect ratio r and axis of

symmetry, \mathbf{m} , a unit vector whose PDF f in time t and space \mathbf{x} is our primary focus.

The physical space we resolve is two-dimensional, including the velocity-gradient direction (y) and the vorticity direction (z). The dimensionless spatial domain is $-1 \leq y \leq 1$, $0 \leq z \leq 1$.

The dimensionless Smoluchowski equation for the PDF $f(\mathbf{m}, \mathbf{x}, t)$ can be written as follows:

$$(1) \quad \begin{aligned} \frac{\partial f}{\partial t} + \mathbf{v} \cdot \nabla f &= R \cdot [Rf + fRV] - R \cdot [\mathbf{m} \times \dot{\mathbf{m}}f], \\ \dot{\mathbf{m}} &= \Omega \cdot \mathbf{m} + a[\mathbf{D} \cdot \mathbf{m} - \mathbf{D} : \mathbf{m}\mathbf{m}\mathbf{m}], \end{aligned}$$

where R is the rotational gradient operator:

$$(2) \quad R = \mathbf{m} \times \frac{\partial}{\partial \mathbf{m}},$$

\mathbf{v} is the fluid velocity, \mathbf{D} and Ω are the rate-of-strain and vorticity tensors,

$$(3) \quad \mathbf{D} = \frac{1}{2}(\nabla \mathbf{v} + \nabla \mathbf{v}^T), \quad \Omega = \frac{1}{2}(\nabla \mathbf{v} - \nabla \mathbf{v}^T),$$

$a = \frac{r^2+1}{r^2-1}$ is the molecular shape parameter. The Doi-Marrucci-Greco potential is

$$(4) \quad V = -\frac{3N_c}{2}\mathbf{M} : \mathbf{m}\mathbf{m} - \frac{1}{2Er}[\Delta \mathbf{M} : \mathbf{m}\mathbf{m} + \theta \nabla \nabla \cdot \mathbf{M} : \mathbf{m}\mathbf{m}],$$

where N_c is a dimensionless nano-particle volume fraction, and θ is a fraction between 0 and 1 that corresponds to equal ($\theta = 0$) or distinct ($\theta \neq 0$) elasticity constants [23]. The second moment tensor \mathbf{M} of f is

$$(5) \quad \mathbf{M} = \mathbf{M}(f) = \int_{|\mathbf{m}|=1} \mathbf{m}\mathbf{m}f(\mathbf{m}, \mathbf{x}, t) d\mathbf{m}.$$

The key dimensionless flow and elasticity parameters are the Deborah (De) and Ericksen (Er) numbers:

$$(6) \quad De = \frac{v_0/h}{D_r^0}, \quad Er = \frac{8}{N_c} \left(\frac{h}{L} \right)^2,$$

where v_0 is the plate speed in the physical experiment, $2h$ is the distance between the two plates, L is the persistence length of distortional elasticity which sets the strength of the distortional elasticity potential, and D_r^0 is the average rotational diffusivity of the spheroidal molecules. The Deborah number describes the bulk plate-imposed shear rate normalized by the molecular relaxation rate, while the Ericksen number measures the strength of the excluded-volume potential relative to distortional elasticity. Slow flows correspond to low De , while highly elastic flows correspond to low Er . Realistic materials have Er on the order of a hundred thousand, which is numerically inaccessible due to highly localized boundary layers which scale with some inverse power of Er ; see the companion paper in this volume ([24]) for a discussion of these structure scaling properties in weak Poiseuille flows.

The Smoluchowski equation (1) is coupled with the dimensionless forms of the balance of linear momentum and continuity equation

$$(7) \quad \begin{aligned} \frac{\partial \mathbf{v}}{\partial t} + (\mathbf{v} \cdot \nabla) \mathbf{v} + \nabla p &= \nabla \cdot \tau_v + \nabla \cdot \tau_e, \\ \nabla \cdot \mathbf{v} &= 0, \end{aligned}$$

where p is the pressure, the stress tensor $\tau = \tau_v + \tau_e$ is given by the constitutive equation [23] which includes both viscous and elastic stresses:

$$\begin{aligned}
 \tau_v &= \mu_3(a)\mathbf{D} + \mu_1(a)(\mathbf{D} \cdot \mathbf{M} + \mathbf{M} \cdot \mathbf{D}) + \mu_2(a)\mathbf{D} : \mathbf{M}_4, \\
 \tau_e &= a\alpha(\mathbf{M} - \frac{\mathbf{I}}{3} - N_c \mathbf{M} \cdot \mathbf{M} + N_c \mathbf{M} : \mathbf{M}_4) \\
 &\quad - a \frac{\alpha}{6Er} (\Delta \mathbf{M} \cdot \mathbf{M} + \mathbf{M} \cdot \Delta \mathbf{M} - 2 \Delta \mathbf{M} : \mathbf{M}_4) \\
 (8) \quad &\quad - \frac{\alpha}{12Er} (2(\Delta \mathbf{M} \cdot \mathbf{M} - \mathbf{M} \cdot \Delta \mathbf{M}) + (\nabla \mathbf{M} : \nabla \mathbf{M} - (\nabla \nabla \mathbf{M}) : \mathbf{M})) \\
 &\quad - a \frac{\alpha \theta}{6Er} [\mathbf{M} \cdot \mathbf{M}_d + \mathbf{M}_d \cdot \mathbf{M} - 4(\nabla \nabla \cdot \mathbf{M}) : \mathbf{M}_4] \\
 &\quad - \frac{\alpha \theta}{6Er} [\mathbf{M}_d \cdot \mathbf{M} - \mathbf{M} \cdot \mathbf{M}_d + (\nabla \nabla \cdot \mathbf{M}) \cdot \mathbf{M} - \mathbf{M}_{\beta j, \alpha} \mathbf{M}_{ij, i}],
 \end{aligned}$$

where the second order tensor \mathbf{M}_d and the fourth moment tensor \mathbf{M}_4 are given by:

$$(9) \mathbf{M}_d = \nabla \nabla \cdot \mathbf{M} + (\nabla \nabla \cdot \mathbf{M})^T, \quad \mathbf{M}_4 = \int_{\|\mathbf{m}\|=1} \mathbf{m} \mathbf{m} \mathbf{m} \mathbf{m} f(\mathbf{m}, \mathbf{x}, t) d\mathbf{m}.$$

The parameter α in the stress tensor measures the strength of entropic relative to kinetic energy, $\mu_i, i = 1, 2, 3$ are three nematic Reynolds numbers.

3. Numerical methods

There are challenges in the numerical simulation of the kinetic model equations, because of nonlocal and nonlinear coupling between flow, short-range and long-range molecular interactions, flow feedback and boundary anchoring conditions. Three different kinds of independent variables appear in the Smoluchowski equation: orientation, space and time. The total number of independent variables is 5 (2 for the orientational configuration space of directions on the unit sphere, 2 for physical space, and 1 for time).

We start with the numerical method developed for monodomain (homogeneous in physical space) Smoluchowski simulations, which reduces to ordinary differential equations in time by modal expansions in spherical harmonics. The dimension of the ODE system depends on the order of truncation of the spherical harmonic expansion. Our studies showed that 65 real amplitudes were necessary to get converged numerical results at the volume fractions of relevance for most nano-composites (on the order of .5 – 5%). For one-dimensional physical space simulations, the Smoluchowski equation transforms to 65 partial differential equations for the spherical harmonic amplitudes; 101 adaptive grid points are used in physical space, necessary to resolve sharp boundary layers whose location is not known *a priori*, and which are furthermore transient (not permanent). Since we also allow for hydrodynamic feedback, the Navier-Stokes equation also was solved, albeit in 1D for our previous codes [25, 12, 11]. Now, we generalize this previous code to solve the Smoluchowski equation in 2 physical space dimensions, time, and full orientational configuration space.

The extension to 2D requires adaptation of numerical technologies for the flow equations. We choose to employ the velocity-pressure formulation of the incompressible Navier-Stokes equation instead of working in the primitive variables. All equations are discretized in space using the method of lines, which yields a large system of ordinary differential equations. To avoid exceedingly large linear algebra solves, we decouple the whole computation into several sub-tasks. First we solve the elliptic equation for the pressure using a multigrid method. Then we update

the velocity in time using the preconditioned Euler method with spectral deferred correction technique; this raises the order of the method to overcome stiff dynamics inherent in these systems. Then we update the Smoluchowski equation again using a preconditioned Euler with spectral deferred corrections, to gain the same order of accuracy.

3.1. Galerkin method for the orientation variable. The orientation variable \mathbf{m} can be expressed in Cartesian coordinates as

$$(10) \quad \mathbf{m} = (\sin \gamma \cos \psi, \sin \gamma \sin \psi, \cos \gamma),$$

where ψ, γ are azimuthal (with respect to the vorticity axis) and polar (in the plane of the flow and flow-gradient) angles, respectively. Instead of discretizing these two angles using grid points on the unit sphere, which may cause singularities at the poles, we resort to numerical approximations of the PDF f by means of the Galerkin spectral technique as we did in the monodomain simulations and in the one-dimensional physical case. The basis functions we choose are spherical harmonic functions, since they are exact normal modes for the rotational diffusion operator when excluded volume is suppressed:

$$(11) \quad Y_l^m(\mathbf{m}) = (-1)^m \sqrt{\frac{(2l+1)(l-m)!}{4\pi(l+m)!}} P_l^m(\cos \gamma) e^{im\psi},$$

$$l = 0, 1, \dots, \quad m = -l, \dots, l,$$

where P_l^m are the associated Legendre polynomials. This choice of basis functions has been pioneered by [18, 5] for rod-like polymers in monodomain simulations for the orientational behavior of the PDF absent of spatial gradients. Let $a_l^m(\mathbf{x}, t)$ denote the (complex) amplitudes of the PDF in the spherical harmonic expansion

$$(12) \quad f(\mathbf{m}, \mathbf{x}, t) \approx \frac{1}{2\sqrt{\pi}} Y_0^0(\mathbf{m}) + \sum_{l=2}^L \sum_{m=-l}^l a_l^m(\mathbf{x}, t) Y_l^m(\mathbf{m}),$$

where the subindex l takes only even integer values because of the reflection symmetry of the PDF $f: f(-\mathbf{m}, \mathbf{x}, t) = f(\mathbf{m}, \mathbf{x}, t)$. (These particles are assumed to be non-polar; for dipolar particles, the dimension essentially doubles.) The Smoluchowski equation (1) is transformed to a large (65 dimensional) system of nonlinear PDEs:

$$(13) \quad \frac{\partial \mathbf{a}}{\partial t} + \mathbf{v} \cdot \nabla \mathbf{a} = \mathbf{F}(\mathbf{a}, \nabla \mathbf{a}, \Delta \mathbf{a}) + \mathbf{G}(\mathbf{a}, \nabla \mathbf{v}),$$

where \mathbf{a} is the vector comprising all unknown amplitudes $a_l^m, l = 2, 4, \dots, L, m = -l, \dots, l$, \mathbf{F} is a nonlinear vector function depending on the amplitudes and their derivatives, and \mathbf{G} is a linear vector function depending on the amplitudes and the divergence of the velocity field.

The accuracy of the numerical approximations of the Smoluchowski equation depends on the truncation of the spherical harmonic expansions. The standard approach since pioneering work of Landau and deGennes [1] has been to model at the scale of light scattering data, namely the second moment tensor of the PDF. Hess and co-workers, Doi, Hinch and Leal, Larson, Forest and Wang, and others have made the connection from the PDF and Smoluchowski equation to second-moment tensor models of Landau-deGennes type. All such models correspond to the extremely low order truncation $L = 2$ with some scheme to achieve closure on the second moments of the PDF. We have shown $L \geq 10$, i.e., at least 65 spherical harmonics, are necessary even in the longwave limit of monodomain simulations

[9, 8]. This calls into question the application of any Landau-deGennes type models for structure simulations, without the backup of a resolved Smoluchowski solver to clean up the potentially significant errors due to under-resolution of the PDF. Indeed, we propose that low-moment models and codes are an important piece of a structure simulation strategy, as a preconditioner and exploration tool that is far less expensive than the code we present here. However, it is not prudent to proceed to design of nano-composite materials without the kinetic solver presented here.

The constitutive equation (8), which enters into the Navier-Stokes solver, involves information from the PDF f . The details are omitted. But we point out that the viscous and elastic stresses only depend on the second and fourth moments, so they are only functions of the second and fourth order harmonic amplitudes (a_2^m , $m = -2, -1, 0, 1, 2$) of f .

3.2. Velocity-pressure formulation. After the decoupling of the flow equation from the Smoluchowski equation, we need to solve the incompressible Navier-Stokes equation (7). There are several numerical methods available. What we use is based on the velocity-pressure formulation [15, 20]. Taking the divergence of the momentum equation and using the incompressible condition, we get an elliptic equation for the pressure. The incompressible Navier-Stokes equation in primitive variables then becomes the velocity-pressure formulation:

$$(14) \quad \frac{\partial \mathbf{v}}{\partial t} + (\mathbf{v} \cdot \nabla) \mathbf{v} + \nabla p = \mu_3 \Delta \mathbf{v} + \nabla \cdot \tau_e$$

$$(15) \quad \Delta p + \nabla v \cdot \frac{\partial \mathbf{v}}{\partial y} + \nabla w \cdot \frac{\partial \mathbf{v}}{\partial z} = \alpha(\mathbf{x}) \nabla \cdot \mathbf{v} + \nabla \cdot (\nabla \cdot \tau_e)$$

where $\mathbf{v} = (u, v, w)$. We follow the idea of Henshaw [15] to add an artificial divergence damping term $\alpha(\mathbf{x}) \nabla \cdot \mathbf{v}$ (with $\alpha(\mathbf{x}) \geq 0$), which is zero theoretically, in the elliptic equation for the pressure p . (For simplicity, we assume $\mu_1 = \mu_2 = 0$ in this paper, and only keep one Reynolds number $\mu_3 \neq 0$.) Under suitable boundary conditions, it has been shown that these two formulations are equivalent.

The velocity-pressure formulation of the Navier-Stokes equation makes it possible to decouple the velocity and the pressure so as to avoid solving large linear systems of equations. In our method, we first solve the elliptic equation (15) for the pressure p using the multigrid method. Then we update the velocity at the new time level by solving the equation (14) using the spectral deferred correction (SDC) method [4] with backward Euler as the basic integration method. Fourth order finite differences are used in the space discretization. The time integration order is 4 by virtue of the SDC method. Slightly more details follow.

3.3. Spatial discretization and time integration. All spatial derivatives in the Smoluchowski equation, constitutive equation, and Navier-Stokes equation are discretized using a standard 4th order centered finite difference method in the interior of the space domain $-1 \leq y \leq 1, 0 \leq z \leq 1$, and the lopsided 4th order finite difference method is used on and near the boundary. In this paper, we use a uniform mesh in both y and z direction. Adaptive meshes will be introduced in the future to capture more complicated structure of the solution.

Using the method of lines, after spatial discretization, we get a large system of ODEs. Because of highly localized (in space and time) structure features in the simulation, the ODEs exhibit severe stiffness. Therefore a good time integrator is required. The spectral deferred correction (SDC) technique [4] can conveniently increase the time integration order. It also preserves the stability property of the

basic integrator. It has proven efficient in our one-dimensional physical space simulations [25, 12], and will again be used here. The basic method in the spectral deferred correction for the Smoluchowski equation is the forward Euler method, while for the velocity equation, we choose the backward Euler method to maintain stability. We continue to work toward an efficient preconditioner for the Smoluchowski equation. Note that after each correction step, the time integration order is increased by 1 until to a maximum order. The quadrature nodes we used in the integration consists of 5 Gauss-Radau nodes, which makes 9 the maximum time integration order [14]. In our computation, three SDC steps are used so that the time integration order is 4.

3.4. Initial and boundary values. Initially, we assume the rod ensemble is in a uniform orientational state across the plate gap, set by the monodomain PDF equilibrium of the Smoluchowski equation. The principal axis of the PDF, the so-called major director, is arbitrary in equilibrium. This degeneracy is broken in confined samples, where the plates impose an anchoring condition on the peak of the PDF, and this is assumed to permeate throughout the sample until the plates are set into motion. Different boundary anchoring conditions on the PDF can be explored in our simulations, but for this initial paper, we choose to align the principal axis of the PDF along the vorticity axis at both boundaries. This is believed to enhance the likelihood of roll-cell instabilities in the flow, as discussed by [6] with a Leslie-Ericksen model and Leal et al. [21, 17] with a second-moment tensor model.

A problem with the velocity-pressure formulation of the incompressible Navier-Stokes equation is the choice of boundary conditions for the velocity and the pressure. The velocity is enforced to be divergence free:

$$(16) \quad u(y=1) = 1, \quad \frac{\partial v}{\partial z}(y=1) = 0, \quad w(y=1) = 0,$$

$$(17) \quad \frac{\partial u}{\partial y}(z=1) = 0, \quad v(z=1) = 0, \quad \frac{\partial w}{\partial y}(z=1) = 0$$

Conditions on other boundaries are similar. More reasonable boundary conditions will be used in future work.

To get the boundary condition for the pressure, we utilize the normal component of the momentum equation which gives

$$(18) \quad \frac{\partial p}{\partial n} = \mathbf{n} \cdot (\mu_3 \Delta \mathbf{v} + \nabla \cdot \tau_M).$$

The initial velocity profile is given by a simple linear shear, which would be the viscous flow profile at sufficiently low Reynolds numbers:

$$(19) \quad \mathbf{v} = (y, 0, 0).$$

4. Numerical results

In this section, we show a preliminary result from the code based on this algorithm. Some parameters are given below: the rod concentration is set at $N_c = 6$ (so the PDF is a nematic Boltzmann-type distribution), very high aspect ratio so that $a \approx 1$, Ericksen number $Er = 500$, Deborah number $De = 15$, effective Reynolds number $\mu_3 = 0.4$. The initial state is logrolling in the whole physical domain domain, i.e., the peak of the PDF is aligned with the vorticity axis. These parameter values are chosen so that the steady experimental conditions lead to a stable steady state. Caution: lowering De or raising Er will lead to dynamic attractor transitions with many pathological features in the flow and PDF. Figure 1 shows the

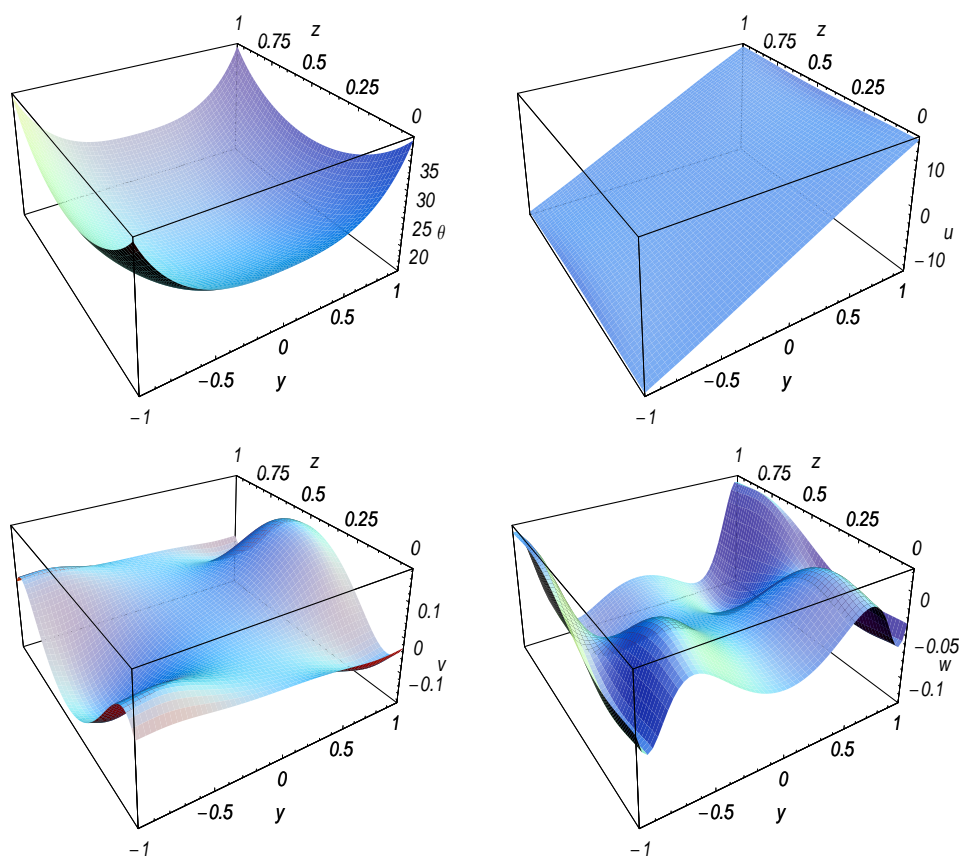


FIGURE 1. Top left: the Leslie angle of the secondary director of the PDF. Top right: the primary velocity component u . Bottom: the velocity components v (left, flow gradient direction) and w (right, vorticity direction), respectively.

final stable structure features. The principal axis of the PDF remains vorticity aligned across the physical domain, which in the monodomain parlance is called a logrolling state (by analogy with logs in a river which align "bank to bank"). Because the major director (the unit eigenvector of the second moment tensor \mathbf{M} corresponding to the largest eigenvalue) is along the vorticity axis, we show in the top-left figure of Figure 1 the Leslie angle (azimuthal angle in the plane of the flow-flow gradient) of the secondary director. A subtle feature of the PDF is captured by this feature: away from the plates, the PDF is no longer uniaxial; the principal values of the second moment \mathbf{M} are all distinct, so there is no longer isotropy in the plane transverse to the principal axis. Thus, there is no secondary boundary angle at the plates; the secondary director is degenerate, without specified direction. It is clearly shown that the Leslie angle has local maxima at the four corners of the physical domain. At the center of the domain, it achieves a minimum. Note that the angle is positive with range $(15^\circ, 40^\circ)$.

Other figures in Figure 1 show the three components of the velocity $\mathbf{v} = (u, v, w)$. Due to the small effective Reynolds number $\mu_3 = 0.4$, the x -component of velocity is almost linear. That is, the flow feedback is minimal along the primary flow

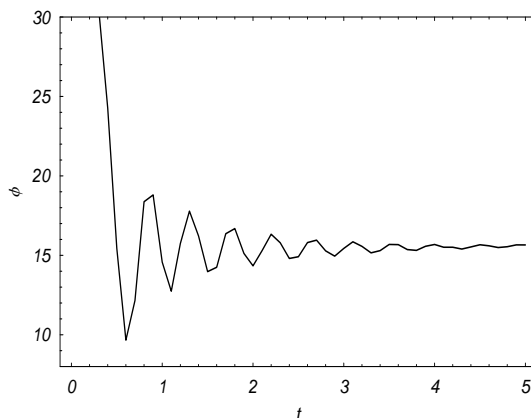


FIGURE 2. The evolution of the Leslie angle for the secondary director in the middle of the computational domain.

component, so that it appears to be a virtual simple linear shear flow. This is consistent with, indeed supports, our 1D simulations [25, 12]. But the other two velocity components do show interesting and new phenomena.

We also show the time evolution of the Leslie angle of the second largest director at the center of the physical domain in Figure 2. It clearly shows that it approaches a stationary stable value with transient, damped oscillations, which is consistent with the transient features of so-called viscous-dominated steady states in our 1D simulations with imposed simple shear flow [12]. This preliminary result provides evidence of stability of these 1D steady structures to higher spatial perturbations in this parameter regime.

5. Conclusion

We have presented a summary of an algorithm for a coupled Smoluchowski-Navier Stokes solver in a confined rectangular domain, with $2D$ spatial resolution, full orientational configuration space resolution, and with a time integrator. This method has been coded and a benchmark simulation is presented for a "fast" flow regime which tends to drive the rod-solvent suspension to steady state. This advance in numerical technology is now poised for exploration of structures and dynamics in the coupling of nano-rod ensembles in a viscous solvent. These PDF databases are then readily transformed to effective property characterization studies.

We submit that this numerical tool is an important piece of a strategy to model nano-composite materials design and control. For this challenge, we have begun collaboration with Max Gunzburger to formulate a control strategy that will require: fast and accurate direct solvers for the processing phase, as presented here; a homogenization or some form of effective property map from the PDF database; and then a performance solver of the elliptic equation with these effective property tensors as variable, anisotropic coefficients. More progress in each phase of the direct problem is clearly needed before we can implement a control formulation.

Acknowledgments

The authors acknowledge financial support from AFOSR grants F49620-03-1-0098, FA9550-05-1-0025, NSF grants DMS-0204243, 0308019, NASA URETI BI-Mat, award No. NCC-1-02037, and the Army Research Office.

References

- [1] P.G. de Gennes and J. Prost. *The Physics of Liquid Crystals*. Oxford University Press, Oxford, 1993.
- [2] E.J. Doedel, A.R. Champneys, T.F. Fairgrieve, Yu.A. Kuznetsov, B. Sandstede, and X. Wang. *AUTO97: Continuation and bifurcation software for ordinary differential equations (with HomCont)*. Technical Report, Concordia University, 1997.
- [3] M. Doi. Molecular dynamics and rheological properties of concentrated solutions of rodlike polymers in isotropic and liquid crystalline phases. *J. Polym. Sci., Polym. Phys. Ed.*, 19:229–243, 1981.
- [4] A. Dutt, L. Greengard, and V. Rokhlin. Spectral deferred correction methods for ordinary differential equations. *BIT*, 40:241–266, 2000.
- [5] V. Faraoni, M. Grosso, S. Crescitelli, and P.L. Maffettone. The rigid-rod model for nematic polymers: An analysis of the shear flow problem. *J. Rheol.*, 43:829–843, 1999.
- [6] J. Feng, J. Tao, and L.G. Leal. Roll cells and disclinations in sheared polymer nematics. *J. Fluid Mech.*, 449:179–200, 2001.
- [7] M.G. Forest and Q. Wang. Monodomain response of finite-aspect-ratio macromolecules in shear and related linear flows. *Rheol. Acta*, 42:180, 2003.
- [8] M.G. Forest, Q. Wang, and R. Zhou. The flow-phase diagram of Doi-Hess theory for sheared nematic polymers II: finite shear rates. *Rheol. Acta*, 44(1):80–93, 2004.
- [9] M.G. Forest, Q. Wang, and R. Zhou. The weak shear phase diagram for nematic polymers. *Rheol. Acta*, 43(1):17–37, 2004.
- [10] M.G. Forest, Q. Wang, R. Zhou, and E. Choate. Monodomain response of arbitrary aspect ratio nematic polymers in general linear planar flows. *J. Non-Newt. Fluid Mech.*, 118(1):17–31, 2004.
- [11] M.G. Forest, R. Zhou, and Q. Wang. Chaotic boundaries of nematic polymers in mixed shear and extensional flows. *Phys. Rev. Lett.*, 93(8):088301, 2004.
- [12] M.G. Forest, R. Zhou, and Q. Wang. Kinetic structure simulations of nematic polymers in plane Couette cells, II: In-plane structure transitions. *SIAM Multiscale Model. Simul.*, 4(4), 2005.
- [13] M. Grosso, R. Keunings, S. Crescitelli, and P.L. Maffettone. Prediction of chaotic dynamics in sheared liquid crystalline polymers. *Phys. Rev. Lett.*, 86:3184, 2001.
- [14] T. Hagstrom and R. Zhou. On the spectral deferred correction of splitting methods for initial value problems. *Comm. App. Math. and Comp. Sci.*, in revision, 2005.
- [15] W.D. Henshaw. A fourth-order accurate method for the incompressible navier-stokes equations on overlapping grids. *J. Comput. Phys.*, 113:13, 1994.
- [16] S. Hess. Fokker-Planck-equation approach to flow alignment in liquid crystals. *Z. Naturforsch Teil*, 31A:1034, 1976.
- [17] D.H. Klein, C. Garcia-Cervera, H.D. Ceniceros, and L.G. Leal. Computational studies of the shear flow behavior of a model for nematic liquid crystalline polymers. *ANZIAM J.*, 46(E):210–244, 2005.
- [18] R.G. Larson and H. Ottinger. The effect of molecular elasticity on out-of-plane orientations in shearing flows of liquid crystalline polymers. *Macromolecules*, 24:6270–6282, 1991.
- [19] R.H. Lusti, P.J. Hine, and A.A. Gusev. Direct numerical predictions for the elastic and thermoelastic properties of short fibre composites. *Composites Sci. Tech.*, 62:1927–1934, 2002.
- [20] N.A. Petersson. Stability of pressure boundary conditions for stokes and navier-stokes equations. *J. Comput. Phys.*, 172:40–70, 2001.
- [21] G. Sgalari, G.L. Leal, and J.J. Feng. The shear flow behavior of lcps based on a generalized doi model with distortional elasticity. *J. Non-Newt. Fluid Mech.*, 102:361–382, 2002.
- [22] R.A. Vaia and E.P. Giannelis. Polymer nanocomposites: Status and opportunities. *MRS Bulletin*, 26(5):394–400, 2001.
- [23] Q. Wang. A hydrodynamic theory for solutions of nonhomogeneous nematic liquid crystalline polymers of different configuration. *J. Chem. Phys.*, 116(20):9120–9136, 2002.
- [24] H. Zhou and M.G. Forest. Nematic liquids in weak capillary poiseuille flow: structure scaling laws and effective conductivity implications. *International J. Numer. Anal. Model.*, 2006.

- [25] R. Zhou, M.G. Forest, and Q. Wang. Kinetic structure simulations of nematic polymers in plane couette cells, I: The algorithm and benchmarks. *SIAM Multiscale Model. Simul.*, 3(4):853–870, 2005.

Department of Mathematics, University of North Carolina at Chapel Hill, Chapel Hill, NC 27599-3250, USA

E-mail: forest@amath.unc.edu

URL: <http://www.amath.unc.edu/Faculty/forest>

Department of Mathematics and Statistics, Old Dominion University, Norfolk, VA 23529, USA

E-mail: rzhou@odu.edu

URL: <http://www.lions.odu.edu/~rzhou>

Department of Mathematical Sciences, Florida State University, Tallahassee, FL 32306, USA

E-mail: wang@math.fsu.edu

URL: <http://www.math.fsu.edu/wang>